Journal of The Electrochemical Society, **166** (4) A641-A648 (2019)
0013-4651/2019/166(4)/A641/8/$38.00 © The Electrochemical Society

Highly Efficient and Non-Precious Metal for the Li-$SOCl_2$ Battery Using Nitrogen Doped Carbon Supported Cu Nanoparticles

Chao Du,[1] Yongji Guan,[1] Shimin Liu,[2] Wenpeng Ni,[2] Junjie Pei,[1] Wei Zhang,[2] Xiaoping Zhang,[1,z] and Youquan Deng[2,z]

[1]*School of Information Science and Engineering, Lanzhou University, Lanzhou 730000, People's Republic of China*
[2]*Centre for Green Chemistry and Catalysis, Lanzhou Institute of Chemical Physics, Chinese Academy of Sciences, Lanzhou 730000, People's Republic of China*

For lithium thionyl chloride batteries, the catalytic activity of the cathode material plays a crucial role in its electrochemical performance. In this paper, a poly (1-vinyl-3-methylimidazolium dicyanamide) ionic liquid (PIL) is selected as precursor to support CuO nanoparticles, and an efficient, non-precious metal nitrogen doped carbon supported Cu nanoparticles (N-C@Cu) composite material is designed and prepared for the lithium thionyl chloride battery cathode catalyst. X-ray diffraction (XRD) and high-resolution transmission electron microscope (HRTEM) verified that the supported CuO nanoparticles is reduced to Cu via carbon which formed from the thermally decompose of PIL. X-ray photoelectron spectroscopy (XPS) images confirm the existence of nitrogen doped carbon and Cu nanoparticles. Raman spectroscopy also demonstrate that the interaction between Cu and N-C provides more active sites. The N-C@Cu composite catalyst exhibits excellent activity in the reduction process of thionyl chloride, as can be seen from the materials display characteristics of lower discharge over-potential, and improved electron transfer of its rate-determining step. The rate performance, operating voltage and discharge capacity are all improved.
 [DOI: 10.1149/2.0701904jes]

Manuscript submitted December 6, 2018; revised manuscript received February 13, 2019. Published March 1, 2019.

Lithium thionyl chloride (Li-$SOCl_2$) battery is well known for its advantages of high operating voltage and high energy density. As a kind of lithium battery, this battery system was comprised of the 1.5 M lithium tetrachloroaluminate in thionyl chloride ($SOCl_2$) used as the electrolyte, the lithium used as the anode and the carbon material such as activated carbon, porous carbon, and acetylene black used as the cathode current collector. Due to its excellent electrochemical performance, for instance stable load voltage, long battery life, and wide temperature application range, it has attracted a lot of attention in aviation, aerospace, navigation and many areas.[1–3] In fact, however, the energy of Li-$SOCl_2$ battery is far below the theoretical value, which seriously hinders its wide application.[4] Later the researchers[5] found that reduction occurred when $SOCl_2$ was adsorbed by the porous carbon cathode: $2SOCl_2 + 4e^- \rightarrow S + SO_2 + 4Cl^-$. The porous carbon cathode material can be used as both a carrier for $SOCl_2$ and a catalyst for the reduction reaction of $SOCl_2$. However, the solid electrolyte interface (SEI) in $SOCl_2$ reduction is slow and cannot support discharge of a large current battery. since the SEI itself cannot be slow, but rather the facility of $SOCl_2$ reduction will define the kinetics. Therefore, in order to improve the electrochemical performance of Li-$SOCl_2$ cells, one possible method is to add a catalyst.[6]

According to previous studies, transition metal macrocyclic compounds are considered to be effective catalysts for the reduction of $SOCl_2$. For example, transition metals (Co, Ni, V, Cu, Mn) complexes of phthalocyanines and porphyrins can effectively catalyze the reduction of $SOCl_2$.[7–9] At the same time, the researchers found that binuclear metal phthalocyanine complexes exhibit more excellent catalytic performance than mononuclear phthalocyanines in Li-$SOCl_2$ cells.[9] A variety of dual-nuclear transition metal macrocyclic compound electrocatalysts are prepared for Li-$SOCl_2$ cells.[10–12] However, the above-mentioned transition metal macrocyclic compounds catalyst is extremely soluble in the electrolyte of the Li-$SOCl_2$ battery. And the soluble transition metal macrocyclic compounds catalysts are deposited at the anode surface by migration, which usually increase the corrosion rate of the lithium anode thus make the anode protective film thicker limiting its practical application.[5] N-doped carbon is then used as a highly efficient electrocatalyst in lithium cells, where N-doped carbon is obtained by thermal decomposition of carbonaceous materials mixed with nitrogen-containing precursors.[13,14] Zheng et al.[15] introduced pyrolyzed N-doped carbon materials, confirming the presence of carbon structural defects and the creation of new active sites after N doping. Liu et al.[16] prepared a N-doped graphene electrocatalyst used in Li-$SOCl_2$ cells by pyrolysis of a mixture of urea and graphene at a high temperature, finally acquiring a certain increase in the working voltage and capacity of the cell. Therefore, it is very necessary to synthesize an insoluble catalyst in the electrolyte which can efficiently catalyze the reduction of $SOCl_2$ with high stability. Thus, many studies focused on developing highly efficient catalysts for the reduction of $SOCl_2$ to significantly reduce the overpotential.

Ionic liquids (ILs) have low volatility, high ion conductivity and excellent thermal stability as room temperature organic salts. And they can be heated without evaporation.[17,18] Poly (ionic liquid) (PIL) is a polymeric material that combines the new properties of ILs, improved dimensional control and mechanical durability of the polymer.[19] PIL has recently been successfully used in the preparation of functional materials and porous nitrogen-doped carbon materials.[20] Moreover, the introduction of nitrogen species plays a crucial role in the outstanding catalytic performance of metal nitrogen carbon catalysts, which can serve as potential promoters for the construction of active sites and regulation of the electronic properties of the catalyst. Meanwhile, Cu has the second highest conductivity (only 6% lower than Ag),[21] which can improve the performance of the active site. Therefore, Cu-contained catalytic materials are widely used in the catalytic industry.[22,23] Cu-based coordination compounds such as Cu(II) phthalocyanine are outstanding redox catalysts both in homogeneous and heterogeneous catalysis reactions.[24] However, the N-doped carbon supported Cu nanoparticles composite materials for $SOCl_2$ reduction has not been reported. Thus, this provides an innovative method for synthesizing stable catalysts for Li-$SOCl_2$ batteries.

In the previous work, we reported[25] that N-doped carbon nanotubes based on ILs precursors was effective cathode catalysts. However, the battery's operating voltage was only 3.39V. In order to further improve the operating voltage of the battery, in this works, we report the synthesis of an efficient and non-precious metal nitrogen doped carbon supported Cu nanoparticles (N-C@Cu) composite material using PIL of the poly (1-vinyl-3-methylimidazolium dicyanamide) salt [VMIm][DCA] to support CuO nanoparticles, and then calcined at 550°C under nitrogen atmosphere when it is used as a cathode catalyst for a non-aqueous Li-$SOCl_2$ battery. At a current density of 10 mA cm^{-2}, the operating voltage can reach 3.48V. Thereinto CuO nanoparticles were reduced to Cu nanoparticles via carbon which formed from the thermally decompose of PIL. The internal resistance of the battery can be reduced due to the introduction of Cu into the composite material. In addition, pyrolysis specific ionic liquids have very low vapor pressure which can take place over a wide temperature range of 400 ~ 1000°C without severe solvent evaporation.[26] Therefore, using ILs as precursors has a significant advantage in terms of composition and

[z]E-mail: zxp@lzu.edu.cn; ydeng@licp.cas.cn

properties of the coating and the adjustment of the interface, which is critical to optimize the design and material. A product of samples was synthesized, namely N-C@Cu, whose loadings in the Ketjenblack (KB) carbon cathode were determined to be 1, 3, 5 and 10 wt%.

Experimental

Materials synthesis.—All the reagents were analytical grade and used without further purification. 1-vinyl-3-methylimidazolium dicyanamide salt [VMIm][DCA] was synthesized based on previous report.[27] In brief, 1-vinylimidazole (10 g, 121.8 mmol) was mixed with 1-methyl bromide (14.6 g, 134 mmol) in a 250 mL flask. The mixture was mega-stirred and heated at 40°C in an oil bath for 24 h. A yellowish material was formed. The compound was dissolved in 50 mL deionized water and then extracted five times using ethyl acetate. The aqueous phase was collected, evaporated in vacuo and placed in a vacuum oven at 50°C for 24 h to remove residual water. The 1-vinyl-3-methylimidazolium bromine (20 g, 104.7 mmol) was dissolved in 250 mL flask with 100 mL deionized water (DI), then the solution of silver dicyanamide (20 g, 115 mmol) was added to it. The slurry was filtered and dried in a vacuum oven at 50°C for 24 h, finally the [VMIm][DCA] was produced.

During the synthesis of the catalyst, the 200 mg of CuO nanoparticles were added to 30 mL of ethanol containing 1 g of [VMIm][DCA]. The excess amount of the ionic liquid monomer was used to completely support CuO nanoparticles. The dispersion was ultrasonicated for 30 min, followed by addition of 35 mg of 2,2'-azobis (isobutyronitrile) (AIBN) to the solution. The solution was then refluxed under a nitrogen atmosphere at 80°C for 24 h.[28] Subsequently, the obtained precursor was calcined in a tube furnace under nitrogen atmosphere at 550°C for 6 h (5°C min^{-1}).[29] The product was denoted as N-C@Cu and under the same conditions, the carbonization of pure PIL was named N-C in this work.

Materials characterization.—The samples were dispersed in KBr granules and tested by FTIR on a Thermo Nicolet 5700 spectrometer. Sample morphology was investigated using a JEM 2010 high resolution transmission electron microscope (HRTEM) operating at 200 k eV. At the same time, the discharge products were subjected to scanning electron microscope (SEM) analysis using a scanning electron microscope (JEOL 6701F) at an accelerating voltage of 5 kV. X-ray diffraction (XRD) patterns were recorded on a powder sample XRD system (Siemens D/mas-RB powder X-ray diffractometer) using Cu Kα radiation (40 mA and 40 kV). The porous structure of the sample was studied using a Micromeritics ASAP 2020 volumetric adsorption analyzer at 76.2 K by using a nitrogen adsorption-desorption isotherm measurement. Based on density functional theory (DFT), pore size distribution is determined from the adsorption branch of the isotherm. The elemental valence state of the sample was investigated for X-ray photoelectron spectroscopy (XPS) using Mg Kα radiation (1253.6 eV) on a VG ESCALAB 210 instrument, and the XPS spectrum was referred to as a C 1s value of 284.6 eV. Raman spectra were measured using a Thermo Nicolet 5700 FT-Raman assisted spectrometer.

Electrochemical characterization.—Cyclic voltammetry (CV) was collected at a voltage sweep rate of 100 mV s^{-1} in a dry environment (water content <1 ppm) using a CHI660A electrochemical workstation with a potential range of 5.0 to 1.0 V (vs. Li / Li^+). Li sheet (1 cm × 1 cm) was used as a counter electrode and reference electrode, and a glassy carbon electrode coated with the catalyst was used as the working electrode to establish a three-electrode system. A $SOCl_2$ solution containing 1.5 M $LiAlCl_4$ was employed as electrolyte (2 mL). Before testing, the glass carbon electrode (Tianjin Ida Tech Co., Ltd; 1mm in diameter) was polished to a mirror surface using 0.05 mm alumina powder on deerskin, cleaned in an ultrasound for 4 min, later dried at 80°C for 6 h. Specifically, 5 mg of the catalyst material was dispersed in 0.5 mL of ethanol containing 20 uL of 5 wt% Nafion solution and ultrasonicated for 30 minutes. Finally, the glass carbon electrode was coated with 3 uL of catalyst containing uniform solution, which was then placed in a dry room with a dew point of -60°C for 1 h to obtain the working electrode for the CV test. For battery testing, the working electrode was made by mixing the KB and polytetrafluoroethylene emulsion (PTFE) with a weight ratio of 5:1. Next, different proportions of N-C@Cu catalyst and a small amount of absolute ethanol were added after agitating for 12 h and was pressed into a 1±0.2 mm thick carbon sheet using a sheet rolling machine. Then the carbon sheet was cut into a round-shaped carbon cathode having a diameter of 10±0.2 mm and dried in an air-drying oven. The Li-$SOCl_2$ battery was assembled in a glove box, wherein water and oxygen levels less than the content of 1ppm. A lithium foil (23mm in diameter) was used as an anode and separated from a glass microfiber filter (Whatman GF/D, 25 mm in diameter). Meanwhile, $SOCl_2$ containing 1.5 M $LiAlCl_4$ was used as the electrolyte, and the water content was controlled to be less than 15 ppm. The battery was typically rested for at least 1 h before measuring a constant current discharge. The galvanostatic discharge test was performed on a LAND battery test system with a current density of 10 mA cm^{-2}. When the battery voltage drops below 2 V, the battery discharge was terminated.

The discharge products were subjected to SEM and XPS tests, first disassembling the batteries in a glove box, and then vacuum drying the carbon electrodes at 80°C. The electrodes were stored in a sealed container, put into the glove box then and finally transferred to a test apparatus.

Results and Discussion

The synthesis process was shown in Fig. 1. After the functionalized IL [VMIm][DCA] was uniformly mixed with the CuO nanopar-

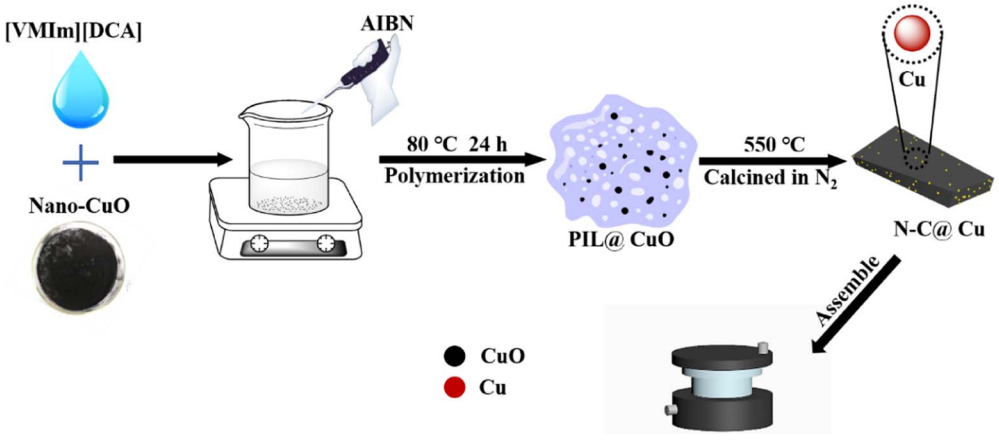

Figure 1. Synthesis strategy of N-C@Cu catalyst and the construction of the Li-$SOCl_2$ cell.

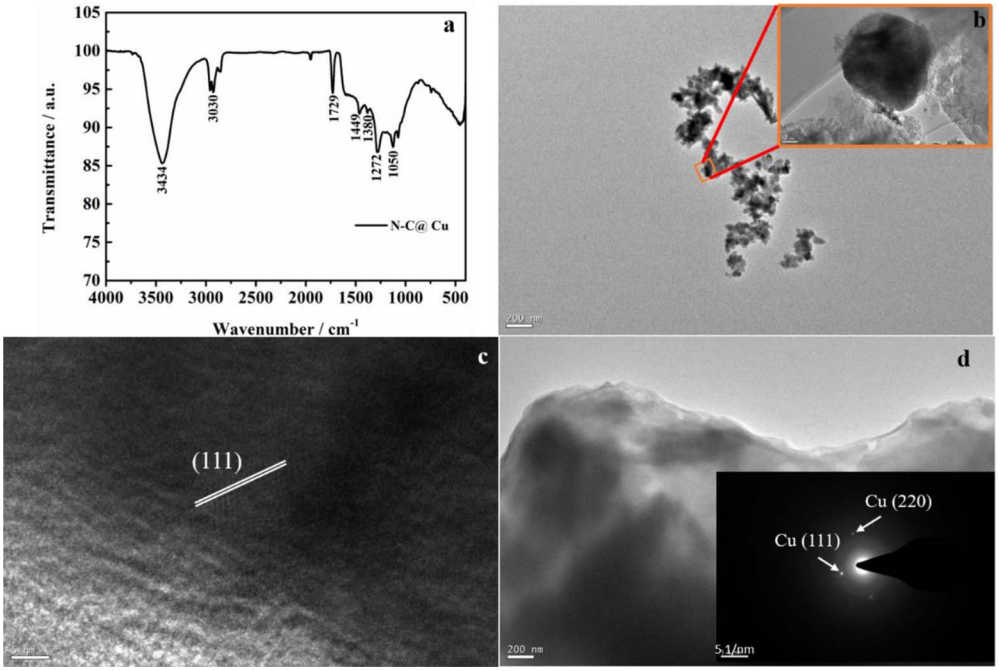

Figure 2. (a) FTIR spectra of N-C@Cu. (b) TEM images of the N-C@Cu. (c) HRTEM images of the N-C@Cu. (d) SEAD pattern (inset) of the N-C@Cu.

ticles, a certain amount of AIBN was added. Then a PIL supported CuO nanoparticles was obtained. Subsequently, the obtained precursor of PIL@CuO was calcined in a tube furnace under nitrogen atmosphere, then the PIL supported CuO nanoparticles was reduced to Cu. As a result, a mesoporous composite namely N-C@Cu was formed and used as a cathode catalytic material of Li-$SOCl_2$ battery.

Characterization of catalysis.—First, the Fig. 2a shows the FTIR spectrum of the N-C@Cu nanoparticles. The peaks at 3434, 1272 and 1050 cm^{-1} are attributed to the characteristic absorption bands of the C-OH stretching vibration mode and the O-H bending vibration mode, respectively.[30] The characteristic absorption band of = C-H stretching at 3030 $cm^{-1}$is also observed,[28] while the peak at 1729 cm^{-1} can be assigned to the C=O-O vibration absorption mode.[31] In addition, the stretching vibration at approximately 1449 cm^{-1} and 1380 cm^{-1} indicates the presence of related nitrogen-containing bonds.[32] Next, the structure of Cu nanoparticles supported with the nitrogen doped carbon was observed by a transmission electron microscope, the structure and morphology of the generated N-C@Cu were also examined. From Fig. 2b, it can be found that the Cu nanoparticles are uniformly supported by the N-C, and N-C@Cu retains the same spherical structure as Cu nanoparticles. The average particle diameter of the supported spherical structure is about 200 nm. At the same time, N-C can be seen as a typical layered structure (Fig. S1). Correspondingly, from the SEAM spectrum in Fig. 2d, diffraction spots attributed to Cu (111) and (220) crystal planes were observed. The crystal lattice spacing of 0.208 nm in the HRTEM image in Fig. 2c is consistent with that of Cu. These results all indicate that the CuO nanoparticles were supported by PIL and in a nitrogen atmosphere at 550°C, CuO was reduced to Cu supported by N-C to form a N-C@Cu structure.

The composition of the catalyst was further examined using XRD, as shown in Fig. 3. In the XRD pattern, the peaks at 35.24°, 38.47°, and 48.58° belong to CuO, and the peak corresponding to N-C is 27.5°, which is consistent with the characteristic peak of N-C that was reported in some literature.[33] At the same time, the structure N-C

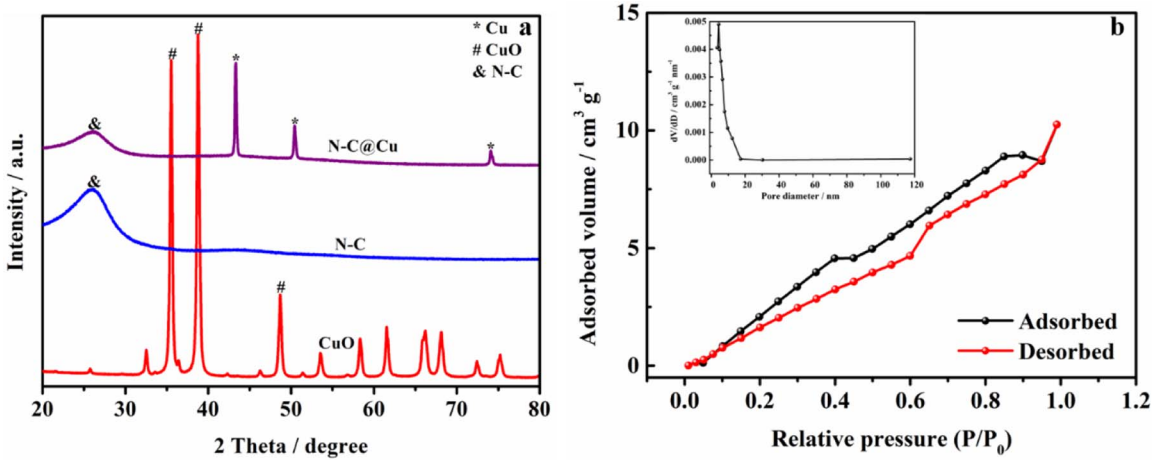

Figure 3. (a) XRD patterns of CuO, N-C, and N-C@Cu. (b) Nitrogen adsorption–desorption isotherms and the pore size distribution (inset) of N-C@Cu.

supported CuO nanoparticles and then formed N-C@Cu at 550°C, the intensity of the peak corresponding to N-C is almost unchanged, but the supported CuO nanoparticles may be reduced to the Cu nanoparticles under nitrogen atmosphere at 550°C for 6 h. Therefore, the peaks at 43.29°, 50.43°, and 74.13° belong to the structure of Cu nanoparticles, while the corresponding peak of CuO is not observed in the structure of N-C@Cu. In addition, the peaks at 43.29° and 74.13° in N-C@Cu are the (111) and (220) diffraction peaks of Cu. The results of XRD and the HRTEM indicate that the CuO nanoparticles undergo a reduction to the metallic state. The presence of the amorphous carbon observed clearly in the HRTEM images suggests[34–36] that PIL thermally decompose to form carbon which acts as a reducing agent to reduce CuO to Cu.[37]

Moreover, it is widely accepted that the surface area and porosity of cathode materials play a vital role in improving the performance of Li-$SOCl_2$ batteries, especially for discharge capacity. Therefore, the N_2 adsorption-desorption measurements were performed to investigate the pore structure of the samples. As shown in Fig. 3b, the nitrogen adsorption-desorption curve of N-C@Cu belongs to type IV, indicating its mesoporous structure. For the N-C@Cu (Table. S1), the specific surface area was 17.41 $m^2\ g^{-1}$, and the pore volume was 0.016 $cm^3\ g^{-1}$. In addition, the pore size distribution shows that the pore size was mostly less than 3.64 nm, which was calculated from the Barrett-Joyner-Halenda (BJH) method. For comparison, the pore structure of commercial CuO and N-C was also tested (Fig. S2), and both samples belong to mesoporous structure. The pore size and pore volume of N-C were 7.16 nm and 0.33 $cm^3\ g^{-1}$, respectively. Obviously, the introduction of Cu nanoparticles has a greater influence on the pore structure of N-C, because Cu nanoparticles derived from CuO in a nitrogen atmosphere at 550°C may block some of the mesopores, resulting in lower pore size and pore volume of N-C@Cu.

X-ray photoelectron spectroscopy (XPS) spectra have been widely used to identify the surface elemental compositions and the chemical state of materials. It can be clearly seen that the overall survey spectrum of the N-C@Cu composite catalytic material (Fig. 4a), indicates the presence of Cu, O, N, and C elements. In the N-C@Cu composite catalytic material (Fig. 4b), the difference between the binding energy of Cu $2p_{3/2}$ (932.9 eV) and Cu $2p_{1/2}$ (952.7 eV) is 19.8 eV,[38] which indicates the presence of Cu nanoparticles. At the same time, in the Cu 2p high-resolution XPS spectrum of CuO (Fig. S3), the difference of binding energy between Cu $2p_{3/2}$ (933.9 eV) and Cu $2p_{1/2}$ (953.9 eV) is 20.0 eV.[39] In the C 1s high-resolution spectrum for N-C@Cu (Fig. 4c), 284.8 eV and 286.8 eV can be fitted, corresponding to carbon atoms[40,41] in C-C and C-N, respectively. Moreover, nitrogen atoms could be detected by the N 1s binding energy, indicating the successful doping of nitrogen atoms into the N-C@Cu. Furthermore, N 1s XPS (Fig. 4d) were discovered with three types of nitrogen in N-C@Cu: pyridinic N (398.6 eV), pyrrolic N (400.4 eV) and quaternary N (401.5 eV), which are ascribed to N-5, N-6 and N-Q, respectively.[42] Thereinto, pyridine nitrogen refers to nitrogen atoms attached to two carbons on the edge of a carbon surface, the atom which has a lone pair of electrons not only provide an electron to the conjugated π bond system but adsorb O_2 molecules and intermediates during the oxygen reduction process to improve the catalytic activity.[43]

Raman spectroscopy can be used to characterize the surface defect formation and graphitization of carbon materials, Raman spectra of N-C and N-C@Cu shown in Fig. 5a. It can be seen from the image that there are two distinct absorption peaks at 1351 cm^{-1} and 1596

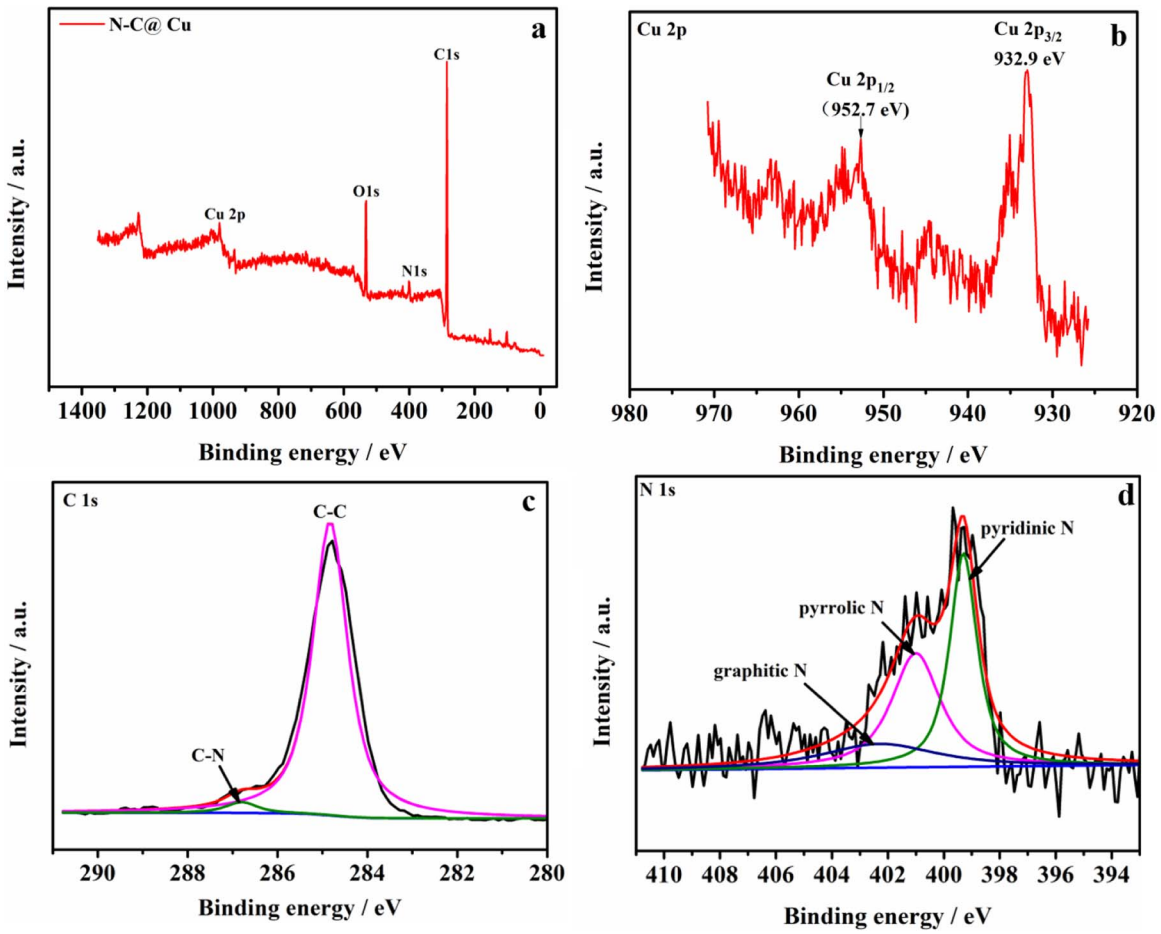

Figure 4. (a) Overall survey spectrum, (b) Cu 2p spectrum, high-resolution (c) C 1s and (d) N 1s spectrum of the N-C@Cu catalyst using an X-ray photoelectron spectroscope.

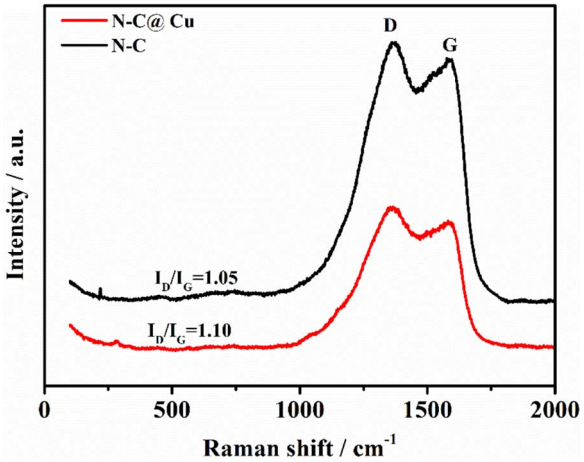

Figure 5. Raman spectroscopy of N-C and N-C@Cu.

cm^{-1} for the two samples. The D peak at 1351 cm^{-1} represents the sp^3 lattice defect presenting in the carbon atom, and the G peak at 1596 cm^{-1} represents the in-plane vibration information of the sp^2 hybridization carbon atom. The ratio of I_D/I_G represents the intensity ratio of the two peaks, which can indicate the degree of defect and disorder of the material.[44,45] The I_D/I_G ratio of the composite catalytic material N-C@Cu (1.10) is higher than that of N-C (1.05). The main reason for this change is that chaos degree increases when Cu particles are introduced into graphitic carbon nitride. At the same time, the interaction between Cu and N-C also provides the material with more active sites.

Electrochemical characterization.—First, the reduction activity of the prepared catalyst in $SOCl_2$ electrolyte containing 1.5M $LiAlCl_4$ was investigated by cyclic voltammetry. As shown in Fig. 6a, there are two reduction peaks in the curve for KB electrode, which shows that two-step electron transfer occurred in the catalytic reaction of the Li-$SOCl_2$ battery.[12] The rate-determining step for the reduction occurring at 2.574 V is shown in Equation 1, and the low current peak at 3.212 V is a fast reaction step as shown in Equation 2.[10]

$$SOCl_2 + e^- \rightarrow 1/2\,SCl_2 + 1/2\,SO_2 + Cl^- \quad [1]$$

$$1/2\,SCl_2 + e^- \rightarrow 1/2\,S + Cl^- \quad [2]$$

There was no related oxidation peak during the reverse scan, which indicates that the reduction of $SOCl_2$ is irreversible.[46] In the electrolyte of 1.5M $LiAlCl_4$, the rate control step potentials of the reduction peaks of CuO and N-C are 2.651 V and 2.661 V, respectively, which are higher than the 2.074 V of pure KB carbon, while N-C@Cu has the highest reduction potential (2.771 V). This indicates that N-C@Cu can effectively improve the reduction of $SOCl_2$. However, the current densities of CuO, N-C and N-C@Cu are lower than that of KB carbon. Meanwhile, as shown in Fig. S4, the Nyquist curve before discharging from a Li-$SOCl_2$ battery containing a pure KB carbon electrode shows that KB carbon has the smallest impedance (5 Ω), which indicates that KB carbon has higher conductivity than these catalysts. As shown in Fig. S5, the current density peak increases slightly as the scan

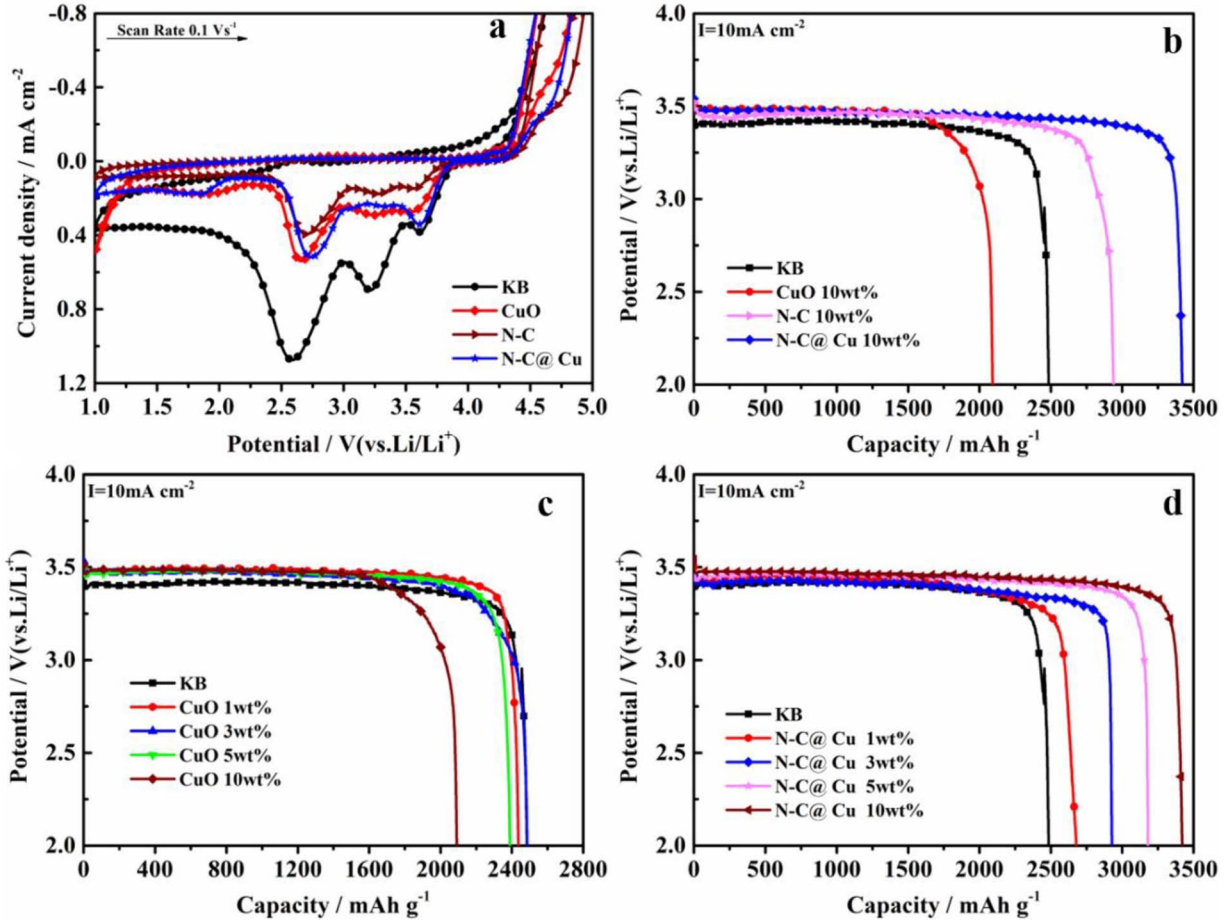

Figure 6. (a) CV curves of KB, CuO, N-C and N-C@Cu in $SOCl_2$ containing 1.5 M $LiAlCl_4$. (b) The discharge curves of Li-$SOCl_2$ batteries with KB, CuO, N-C, and N-C@Cu electrodes at the current density of 10mA cm^{-2}. The discharge curves of Li-$SOCl_2$ batteries containing different amounts of catalysts (c) CuO, (d) N-C@Cu.

rate increases, and the reduction peak potential gradually moves to negative potential. By studying the kinetic process, it was shown that the reaction is not affected by the mass transfer process, but rather linear relationship between current density and scanning speed.[47]

Based on the performance of the Li-$SOCl_2$ battery containing these catalysts, a current density of 10 mA cm^{-2} was used in the voltage range of 2 to 3.6 V to conduct the test. CuO and N-C were added as the catalyst to the KB carbon that was used as the cathode material of the Li-$SOCl_2$ battery (Fig. 6b). Compared with the pure KB carbon electrode (2484 mAh g^{-1}), the discharge capacity (2092 mAh g^{-1}) of CuO is lower than that of KB carbon, while the discharge capacity of N-C is 2938 mAh g^{-1}. At the same time, when N-C@Cu was added as a catalyst to KB carbon, the maximum discharge capacity was 3419 mAh g^{-1}, which indicate that N-C@Cu can effectively catalyze the reduction of $SOCl_2$. These results are also consistent with the cyclic voltammetry test of the electrodes. However, as the catalyst content increases, the discharge capacities of CuO and N-C@Cu cells show different trends, as shown in Figs. 6c and 6d. When the content of CuO is increased to 5 wt%, the discharge capacity of the battery is almost equivalent to the discharge capacity of pure KB carbon, and the operating voltage has a significant increase (100 mV). In particular, when the content of CuO was increased to 10 wt%, the discharge capacity was reduced to 2092 mAh g^{-1}, which was mainly due to excessive CuO added to KB carbon blocking the pore structure of the carbon cathode,[10] resulting in a decrease in discharge capacity. However, as the catalyst content increases, the discharge capacity of N-C@Cu cells sequentially increases. When the content of N-C@Cu is 10 wt%, the maximum discharge capacity is 3419 mAh g^{-1}, which proves that N-C@Cu is a novel catalyst different from CuO. All these indicate that N-C@Cu is more advantageous than pure KB carbon electrode as a cathode catalyst for Li-$SOCl_2$ battery.

The study of the rate performance of N-C@Cu catalysts shows that both the discharge capacity and the discharge voltage gradually decrease as the current density increases. High current discharge can form enough LiCl and element S in a short time to block the pore structure in the carbon cathode of the Li-$SOCl_2$ cell, which explains its reduced capacity at high currents. At the same time, LiCl deposited on the surface of the electrode increases the internal resistance of the battery, causing the discharge voltage of the battery to decrease. As shown in Fig. 7, all currents have a good discharge platform at a current density of 10∼40 mA cm^{-2}. As shown in Fig. 7c, when the current density is increased to 20 mA cm^{-2}, the capacities of KB and N-C@Cu are 82.9% and 92.8% of the initial capacity. What's more, when the current density is increased to 40 mA cm^{-2}, the capacity of KB and N-C@Cu are only 55.6% and 41.7% of the initial capacity, respectively. These show that when N-C@Cu is used as a cathode catalyst for Li-$SOCl_2$ cells, it has more advantages than pure KB carbon electrodes at low current density ($I <= 25$ mA cm^{-2}). In contrast, the advantages of pure KB carbon are even more pronounced at high current densities. We can explain this phenomenon reasonably with the following fact that after adding a certain mass fraction of N-C@Cu catalyst to the pure KB carbon, the pore structure of the carbon cathode changes. Further, Fig. 7d shows the N-C@Cu the more stable variation of work voltage than KB at different current densities during the rate performance test.

In the discharge process, the active material $SOCl_2$ is adsorbed on the surface of the carbon electrode to generate S and SO_2 through the disproportionation reaction, in which the catalytic process of $SOCl_2$ reduction was described.[16] The O atom in $SOCl_2$ adsorbs onto C^x to

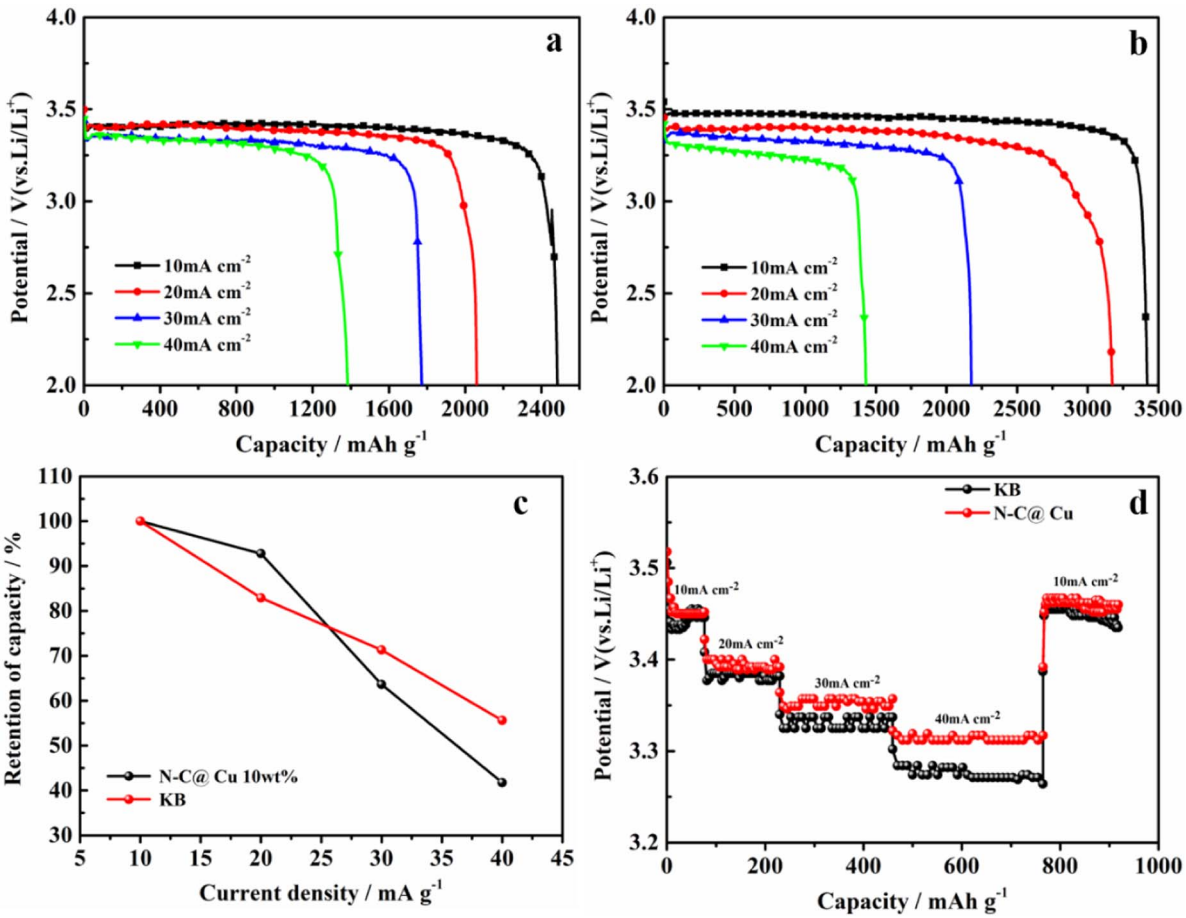

Figure 7. The discharge profiles of Li-$SOCl_2$ batteries at different current density for (a) KB, (b) N-C@Cu. (c) The capacity retention capability of Li-$SOCl_2$ batteries with N-C@Cu and KB electrodes at various current densities. (d) Comparison of rate performance of KB and N-C@Cu at various current densities.

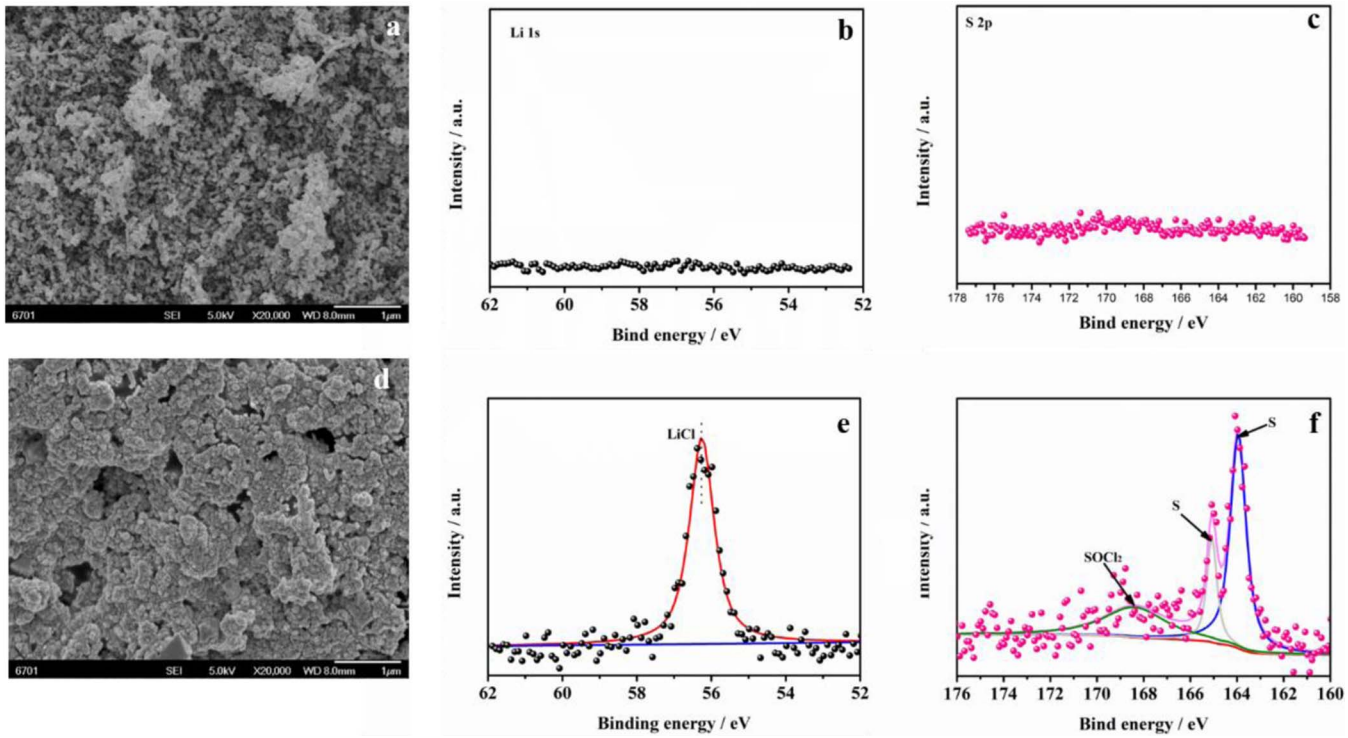

Figure 8. SEM images of the N-C@Cu electrode (a) before discharge, (d) after discharge. The high-resolution Li 1s spectrum of the N-C@Cu electrode (b) before discharge, (e) after discharge. The high-resolution S 2p spectrum of the N-C@Cu electrode (c) before discharge, (f) after discharge.

form the $SOCl_2$ C^x adduct. Next, the adduct receives an electron from N^{x-}, $SOCl_2$ is reduced to $1/2SCl_2$, $1/2SO_2$ and Cl^-. The S in SCl_2 adsorbs onto C^x to form the $1/2SCl_2{\cdot}C^x$ adduct, and then $1/2SCl_2{\cdot}C^x$ immediately received another electron from N^{x-} to form 1/2S and Cl^-. Meanwhile, the introduction of Cu nanoparticles may reduce the internal resistance of the battery, thereby further increasing the operating voltage of the battery. The catalytic process in which $SOCl_2$ is reduced is as follows:

$$C^x + SOCl_2 \rightarrow C^x{\cdot}SOCl_2 \quad [3]$$

$$C^x{\cdot}SOCl_2 + e^-_{N_x} \rightarrow 1/2\,SCl_2{\cdot}C^x + 1/2SO_2 + Cl^- \quad [4]$$

$$1/2\,SCl_2 + C^x \rightarrow 1/2\,SCl_2{\cdot}C^x \quad [5]$$

$$1/2\,SCl_2{\cdot}C^x + e^-_{N_x} \rightarrow 1/2\,S + Cl^- \quad [6]$$

Characterization of discharge products.—Next, the morphologies of the electrodes at various stages were studied using scanning electron microscopy. Meanwhile, the sulfur and lithium species on the surface of the electrode were analyzed using XPS Li 1s and S 2p spectra. For the N-C@Cu electrode, the particles on the electrode before the discharge are relatively smooth and loose (Fig. 8a), and no peak observed from Li 1s XPS spectrum (Fig. 8b) and S 2p XPS spectrum (Fig. 8c). As shown in Fig. 8d, the pore structure in the electrode surface after discharge was almost covered by the discharge product and the surface was relatively dense. While the XPS results of Figs. 8e and 8f showed that the discharge products were mainly LiCl and S[(48)] with a small amount of $SOCl_2$, which was adsorbed by electrode material. It is worth noting that, for N-C@Cu electrode, the content of LiCl and S products is higher than that of the pure KB carbon electrode after discharging (Fig. S6c and S6d). Unlike pure KB electrodes (Fig. S6a and S6b), the discharge products formed on the N-C@Cu electrode have larger particle agglomeration. These results have yet again demonstrated that N-C@Cu composites can promote the reduction of $SOCl_2$ in Li-$SOCl_2$ batteries compared to pure KB carbon electrode.

Conclusions

In summary, N-C@Cu composite catalyst was prepared, characterized and used as a cathode catalyst in a non-aqueous Li-$SOCl_2$ battery, which displayed high catalytic activity in the reduction of $SOCl_2$. At a current density of 10 mA cm^{-2}, the discharge capacity can reach 3419 mAh g^{-1} and the operating voltage can reach 3.48V. Meanwhile, it has been enhanced in terms of battery performance such as rate performance and discharge stability. The high activity of the catalyst benefits from the strong catalytic ability of nitrogen doped carbon itself and the high conductivity of Cu. Therefore, the possible interaction between N-C@Cu and $SOCl_2$ and the more contact sites of the catalyst reduce its overpotential potential, thereby improving the overall performance of the battery. However, the longer-term stability of the catalyst should be further verified in the future works.

Acknowledgments

The authors acknowledge the financial support of this work from the Fundamental Research Funds for the Central Universities (Nos. lzujbky-2018-it62) and (Nos. lzujbky-2018-129), and the Science and Technology support program of Gansu Province (Nos.18JR3RA297).

ORCID

Youquan Deng https://orcid.org/0000-0002-7612-0354

References

1. J. Li, C. Daniel, and D. Wood, *J. Power Sources*, **196**, 2452 (2011).
2. W. C. West, A. Shevade, J. Soler, J. Kulleck, M. C. Smart, B. V. Ratnakumar, M. Moran, R. Haiges, K. O. Christe, and G. K. S. Prakash, *J. Electrochem. Soc.*, **157**, A571 (2010).
3. X. Q. Su, J. Li, G. P. Yao, J. L. Wang, J. S. Zhao, and F. X. Zhang, *Catal. Commun.*, **37**, 23 (2013).
4. R. Zhang, J. Wang, B. Xu, X. Huang, Z. Xu, and J. Zhao, *J. Electrochem. Soc.*, **159**, H704 (2012).
5. B. Li, Z. Yuan, Y. Xu, and J. Liu, *Electrochim. Acta*, **217**, 73 (2016).
6. S. B. Lee, S. I. Pyun, and E. J. Lee, *Electrochim. Acta*, **47**, 855 (2001).

7. K. M. Abraham, M. Alamgir, and W. P. Kilroy, *J. Power Sources*, **26**, 597 (1989).
8. R. J. Nowak, D. R. Rolison, J. J. Smith, and S. Szpak, *Electrochim. Acta*, **33**, 1313 (1988).
9. S. P. Huang and Z. Z. Yuan, *Acta Phys. Chim. Sin.*, **25**, 1599 (2009).
10. R. Zhang, B. Xu, J. Wang, J. Zhao, and S. Zhang, *J. Mater. Res.*, **29**, 793 (2014).
11. R. Guo, Z. Dong, B. Xu, C. Song, Z. Li, J. Zhao, and S. Zhang, *ECS. electrochem. lett*, **3**, A36 (2014).
12. Z. Liu, Q. Jiang, R. Zhang, R. Gao, and J. Zhao, *Electrochim. Acta*, **187**, 81 (2016).
13. R. Wu, S. Chen, Y. Zhang, Y. Wang, W. Ding, L. Li, X. Qi, X. Shen, and Z. Wei, *J. Power Sources*, **274**, 645 (2015).
14. L. Zhao, L. Z. Fan, M. Q. Zhou, H. Guan, S. Qiao, M. Antonietti, and M. M. Titirici, *Adv Mater*, **22**, 5202 (2010).
15. B. Zheng, J. Wang, F.-B. Wang, and X.-H. Xia, *Electrochem. Commun.*, **28**, 24 (2013).
16. B. Li, Z. Yuan, Y. Xu, and J. Liu, *Appl. Catal., A*, **523**, 241 (2016).
17. L. Qiu, B. Liu, Y. Peng, and F. Yan, *Chem Commun (Camb)*, **47**, 2934 (2011).
18. X. Chen, Q. Li, J. Zhao, L. Qiu, Y. Zhang, B. Sun, and F. Yan, *J. Power Sources*, **207**, 216 (2012).
19. B. Lin, L. Qiu, J. Lu, and F. Yan, *Chem.mater.*, **22**, 6718 (2010).
20. J. S. Lee, X. Wang, H. Luo, and S. Dai, *Adv Mater*, **22**, 1004 (2010).
21. R. Wang and H. Ruan, *J. Alloys Compd.*, **656**, 936 (2016).
22. M. A. Thorseth, C. E. Tornow, E. C. M. Tse, and A. A. Gewirth, *Coord. Chem. Rev.*, **257**, 130 (2013).
23. M. S. Thorum, J. Yadav, and A. A. Gewirth, *Angew. Chem. Int. Ed.*, **48**, 165 (2009).
24. M. B. Gawande, A. Goswami, F. X. Felpin, T. Asefa, X. Huang, R. Silva, X. Zou, R. Zboril, and R. S. Varma, *Chem Rev*, **116**, 3722 (2016).
25. C. Du, S. Liu, W. Zhang, X. Zhang, and Y. Deng, *J. Electrochem. Soc.*, **165**, A1955 (2018).
26. M. Nguyen, L. Nguyen, E. Jeon, J. Kim, M. Cheong, H. Kim, and J. Lee, *J. Catal.*, **258**, 5 (2008).
27. P. Li, D. R. Paul, and T.-S. Chung, *Green. Chem.*, **14**, 1052 (2012).
28. W. Ni, S. Liu, Y. Fei, Y. He, X. Ma, L. Lu, and Y. Deng, *ACS Appl Mater Interfaces*, **9**, 14749 (2017).
29. W. J. Ong, L. L. Tan, Y. H. Ng, S. T. Yong, and S. P. Chai, *Chem Rev*, **116**, 7159 (2016).
30. W. Lu, X. Qin, S. Liu, G. Chang, Y. Zhang, Y. Luo, A. M. Asiri, A. O. Al-Youbi, and X. Sun, *Anal Chem*, **84**, 5351 (2012).
31. L. Zhou, Y. Lin, Z. Huang, J. Ren, and X. Qu, *Chem Commun (Camb)*, **48**, 1147 (2012).
32. M. Zhang, L. Bai, W. Shang, W. Xie, H. Ma, Y. Fu, D. Fang, H. Sun, L. Fan, M. Han, C. Liu, and S. Yang, *J. Mater. Chem.*, **22**, 7461 (2012).
33. J. Liu, T. Zhang, Z. Wang, G. Dawson, and W. Chen, *J. Mater. Chem.*, **21**, 14398 (2011).
34. M. J. Siegfried and K. S. Choi, *J Am Chem Soc*, **128**, 10356 (2006).
35. D. S. Jacob, I. Genish, L. Klein, and A. Gedanken, *The journal of physical chemistry. B*, **110**, 17711 (2006).
36. D. S. Jacob, L. Bitton, J. Grinblat, I. Felner, Y. Koltypin, and A. Gedanken, *Chem.mater.*, **18**, 3162 (2006).
37. L. X. Yang, Y. J. Zhu, W. W. Wang, H. Tong, and M. L. Ruan, *The journal of physical chemistry. B*, **110**, 6609 (2006).
38. S. H. Noh, M. H. Seo, X. Ye, Y. Makinose, T. Okajima, N. Matsushita, B. Han, and T. Ohsaka, *J. Mater. Chem. A.*, **3**, 22031 (2015).
39. X. Han, X. He, L. Sun, X. Han, W. Zhan, J. Xu, X. Wang, and J. Chen, *ACS Catalysis*, **8**, 3348 (2018).
40. S. Liu, J. Tian, L. Wang, Y. Luo, J. Zhai, and X. Sun, *J. Mater. Chem.*, **21**, 11726 (2011).
41. Z. Lin and X. Wang, *Angew. Chem. Int. Ed.*, **52**, 1735 (2013).
42. C. Pan, L. Qiu, Y. Peng, and F. Yan, *J. Mater. Chem.*, **22**, 13578 (2012).
43. T. C. Nagaiah, S. Kundu, M. Bron, M. Muhler, and W. Schuhmann, *Electrochem. Commun.*, **12**, 338 (2010).
44. J. Jiang, L. Ou-yang, L. Zhu, A. Zheng, J. Zou, X. Yi, and H. Tang, *Carbon*, **80**, 213 (2014).
45. Q. Liang, Z. Li, X. Yu, Z. H. Huang, F. Kang, and Q. H. Yang, *Adv Mater*, **27**, 4634 (2015).
46. K. M. Abraham, M. Alamgir, and S. J. Perrotti, *J. Electrochem. Soc.*, **135**, 2686 (1988).
47. X. Li, X. Huang, R. Gao, R. Zhang, and J. Zhao, *Electrochim. Acta*, **222**, 203 (2016).
48. V. P. Zakaznova-Herzog, S. L. Harmer, H. W. Nesbitt, G. M. Bancroft, R. Flemming, and A. R. Pratt, *Surface Science*, **600**, 348 (2006).